Comparison of airborne and spaceborne 95-GHz radar reflectivity and evaluation of multiple scattering effects in spaceborne Measurements

D. Bouniol, Alain Protat, Artemio Plana-Fattori, Manuel Giraud, Jean-Paul Vinson, Noël Grand

Comparison of Airborne and Spaceborne 95-GHz Radar Reflectivities and Evaluation of Multiple Scattering Effects in Spaceborne Measurements

DOMINIQUE BOUNIOL

Centre National de la Recherche Météorologique/GAME, Météo-France/CNRS, Toulouse, France

ALAIN PROTAT, ARTEMIO PLANA-FATTORI, MANUEL GIRAUD, AND JEAN-PAUL VINSON

Centre d'Étude des Environnements Terrestre et Planétaires, Vélizy, France

NOËL GRAND

Division Technique, INSU, Meudon, France

(Manuscript received 3 April 2007, in final form 21 March 2008)

ABSTRACT

This paper provides an evaluation of the level 1 (reflectivity) *CloudSat* products by making use of coincident measurements collected by an airborne 95-GHz radar during the African Monsoon Multidisciplinary Analysis (AMMA) experiment that took place in summer 2006 over West Africa. In a first step the airborne radar calibration is assessed. Collocated measurements of the spaceborne and airborne radars within the ice anvil of a mesoscale convective system are then compared. Several aspects are interesting in this comparison: First, both instruments exhibit attenuation within the ice part of the convective system, which suggests either the presence of a significant amount of supercooled liquid water above the melting layer or the presence of wet and very dense ice. Second, from the differences in the observed reflectivity values, a multiple scattering enhancement of at least 2.5 dB in the *CloudSat* reflectivities at flight altitude is estimated. The main conclusion of this paper is that in such thick anvils of mesoscale convective systems the *CloudSat* measurements have to be corrected for this effect, if one wants to derive accurate level 2 products such as the ice water content from radar reflectivity. This effect is expected to be much smaller in nonprecipitating clouds though.

1. Introduction

The African Monsoon Multidisciplinary Analyses (AMMA) experiment's special observing period (SOP) 3 took place between 15 and 30 September 2006 in the Dakar region of Senegal. Among other scientific objectives, this SOP was devoted to the investigation of the evolution of microphysical properties of mesoscale convective systems as they arrive in the coastal environment and to the evaluation of the *CloudSat–Cloud-Aerosol Lidar and Infrared Pathfinder Satellite Observations* (*CALIPSO*) satellite constellation's level 1 and 2 products within this particular region of West Africa. This tandem of active sensors (95-GHz radar and dual-wavelength lidar) had indeed been successfully launched in April 2006 to investigate cloud properties at global scale. The time frame of the AMMA campaign was particularly well suited for the *CloudSat–CALIPSO* validation, and represented a major opportunity for the scientific product evaluation in this particular region, where operational data are usually sparse.

To fulfill these objectives, the French Falcon 20 (F-F20) was deployed with a 95-GHz Doppler radar and a three-wavelength lidar, therefore replicating the spaceborne payload, as well as a set of standard microphysical instrumentation [two-dimensional 0.2-mm-resolution precipitation (2D-P) probe, two-dimensional 0.25-mm-resolution cloud (2D-C) probe, Forward Scattering Spectrometer Probe (FSSP), and one-dimensional 0.2-mm-resolution precipitation (1D-P) probe], covering the whole cloud particle size range, and the dropsonde capability. Flight strategies were designed to first underfly the National Aeronautics and Space Administration (NASA)–Centre National D'Études Spatiales

Corresponding author address: Dominique Bouniol, CNRM/GMME, Météo-France, 47 Ave. Gaspard Coriolis, 31057 Toulouse CEDEX, France.
E-mail: dominique.bouniol@meteo.fr

DOI: 10.1175/2008JTECHA1011.1

TABLE 1. RASTA system specifications during the AMMA experiment. The antennas referred to as "down-back" and "up-back" are the downward-looking and upward-looking antennas, both pointing 38° off-nadir and in the direction opposite to the aircraft heading. The "down-trans" antenna is downward-looking, pointing 20° off-nadir, and in the direction perpendicular to the aircraft heading.

Frequency (GHz)			95.04		
Peak power (kW)			1.8		
PRF (kHz)			10		
Pulse width (μs)/gate length (m)			0.4/60		
Transmit polarization			H		
Receive polarization			H		
Minimum detectable range (m)			240		
	Nadir	Down-back	Down-trans	Zenith	Up-back
Antenna gain (dB)	47	47	47	47	41
Antenna beamwidth (°)	0.7	0.7	0.7	0.7	1.4
Antenna size (cm)	30	30	30	30	15
Real-time processing			Pulse pair		

(CNES) Afternoon Satellite Constellation (A-Train) track and to then document the cross-track variability. Such datasets will be particularly useful for the validation of upcoming new methods combining active and passive sensors of the A-Train.

The new Radar Aéroporté et Sol de Télédétection des Propriétés Nuageuses (RASTA) radar was implemented for the first time in a field campaign during AMMA. Table 1 shows the radar characteristics during AMMA. Its major improvement compared to the previous version (Protat et al. 2004) is the implementation of a cluster of five antennas (three downward, two upward) allowing for the retrieval of the three-dimensional wind field in a vertical cross section below the aircraft track and the two-dimensional wind field in a vertical cross section above flight level. The emission is switched from one antenna to the next every 0.5 ms. As a result, the horizontal resolution of the measurements for each of the five antennas is 2.5 s (or 500 m for an aircraft flying at 200 m s^{-1}).

To accurately assess the level 1 *CloudSat* reflectivities, a flight was dedicated to evaluate the RASTA calibration. The basic idea is first to evaluate the calibration of the nadir-looking antenna and then to propagate this calibration to the four other antennas by comparing statistically the reflectivities of the five antennas for the gates closest to the aircraft. The details of the calibration procedure are given in the following section. A comparison of reflectivities measured by RASTA and *CloudSat* is then undertaken in section 3. Concluding remarks are given in section 4.

2. Calibration of the nadir-looking antenna of the 95-GHz airborne radar

Flight 78 (28 September 2006) was dedicated to the evaluation of the calibration of the RASTA radar. A first calibration proxy has been obtained from ground-based measurements prior to its implementation on board the aircraft. It has then been chosen to follow the calibration procedure proposed by Li et al. (2005) and to calibrate the radar reflectivity using the ocean surface backscattering (σ_0). By minimizing the different factors that affect the measurements of σ_0 (i.e., the surface wind, the attenuation due to atmospheric gases, the beam filling at the surface, and the variation of the Fresnel reflection coefficient), the calibration of a 95-GHz radar can be achieved with an accuracy of around 1–2 dBZ. As stated in Li et al. (2005), the main error that can affect the σ_0 measurement is the estimation of the two-way attenuation, and they recommend performing this type of calibration in favorable atmospheric conditions (i.e., midlatitude ocean during winter). Under such conditions, the two-way path-integrated attenuation (PIA) is about 1 dB whereas for tropical oceans it can be as large as 6 dB. To overcome this problem, three sondes were launched during flight 78 in order to accurately document the atmospheric profiles and to compute the two-way PIA through an attenuation model.

Figure 1 (left) depicts the F-F20 flight track on 28 September 2006. The flight has been divided into segments, as seen in Fig. 1 (right), that shows the flight altitude, roll, and pitch as a function of time. A proper definition of pitch and roll angles can be found in Testud et al. (1995). The RASTA radar is not a permanent fixture on the F-F20. Therefore, the mounting angles of the antennas must be checked to ensure that they are accurately estimated. The radar is mounted using a negative pitch (directed to the rear of the aircraft) in order to compensate for the natural in-flight pitch angle of the aircraft. By including this angle, it is expected that if the aircraft flies straight-line patterns without any roll, the radar beam will sample in the

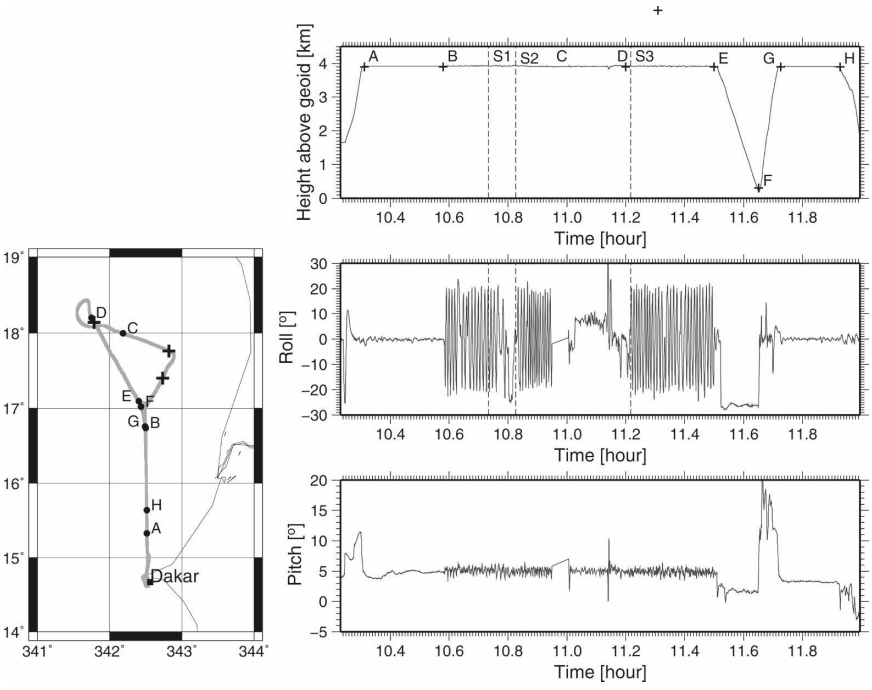

FIG. 1. (left) Flight track performed on 28 Sep 2006. The crosses show the dropsonde launching positions. (right) Flight parameters: altitude, roll, and pitch (from top to bottom) as a function of time.

exact nadir direction. The A–B segment corresponds to the flight track that has been used, keeping the roll as close as possible to zero, in order to find the pitch angle for which the Doppler velocity at ground level is as close as possible to zero (since in this situation the radar measures the vertical velocity of the ground). This exact null velocity at ground level is quite difficult to achieve due to the large aircraft speed contamination of the Doppler measurement. Indeed, due to aircraft speed (about 200 m s^{-1}), a very small incidence angle will lead to a Doppler velocity at ground level that is different from zero. However, after a careful processing of the Doppler observations, this null Doppler velocity is observed for a pitch angle of 4.75° (not shown), corresponding to the deviation of the nadir beam to the rear of the aircraft. This value has been retained in the following in order to compute the real incidence angle of the radar beam.

The B–C and D–E segments of the flight correspond to the measurements of σ_0 at different incidence angles, as can be observed in the roll time series. By plotting the reflectivity measurements at the ocean surface as a function of the roll angle for these segments (where the pitch has been set close to 4.75°, but cannot be kept strictly constant due to aircraft motions), a symmetric patterns of behavior of the reflectivity values around the 0° roll line is found, leading to the conclusion that the roll is not affected by antenna-mounting error.

The E–F segment consists of a Lagrangian descent in order to obtain a thermodynamical description of the lower troposphere using the in situ measurements at flight level. Finally, S1, S2, and S3 (crosses in the left-hand panel of Fig. 1 or the vertical dashed line in the right-hand side panel) correspond to the three locations where dropsondes were launched.

a. Estimation of the two-way PIA

Li et al. (2005) have stressed that reliable atmospheric attenuation estimates are required for the proper calibration of an airborne radar operating at a frequency near 95 GHz, because attenuation caused by water vapor and oxygen can be significant in such a frequency domain. In the present study, attenuation due to water vapor and oxygen is assessed from the atmospheric profiles provided by the above-mentioned dropsondes.

Attenuation calculations at 95.04 GHz were performed through the model developed by Liebe et al. (1993). The imaginary part of the complex refractivity was computed as the sum of the contributions associated with molecular oxygen (pressure-broadening and nonresonant terms) and water vapor (pressure broadening and continuum). Results from this model can differ from those provided by the model proposed by Ulaby et al. (1981), which includes a simpler representation of the relevant attenuation. Under relatively

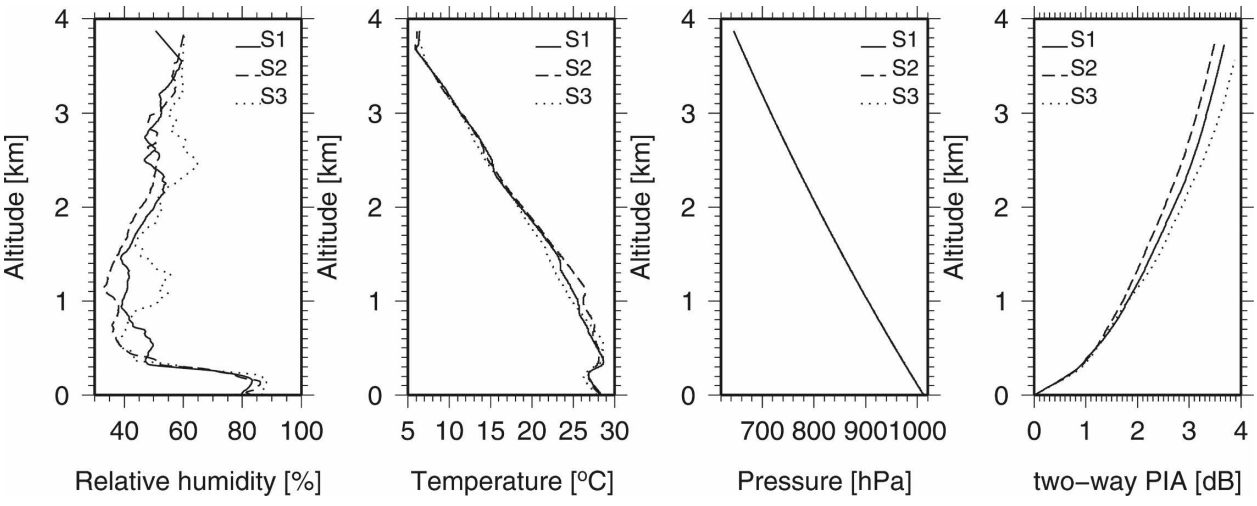

FIG. 2. (left to right) Relative humidity, air temperature and pressure, and resulting two-way attenuation estimates, at the points S1, S2, and S3 in Fig. 1, where the three dropsondes were released on 28 Sep 2006.

warm and moist atmospheric conditions [e.g., the tropical model presented by Ellingson et al. (1991)], the Ulaby et al. (1981) model overestimates by 0.2 dB the two-way PIA provided by the Liebe et al. (1993) model for a nadir-viewing airborne radar at 95 GHz flying at 4 km.

All of the available dropsonde observations of relative humidity, air temperature, and pressure were taken into account. Resulting two-way PIA profiles (Fig. 2) are slightly different from each other, as a consequence of the spatial variability associated with the humidity and temperature profiles over the area under consideration. Two-way PIA values at the aircraft level were 3.7, 3.5, and 3.9 dB, respectively. Because of the spatial variability and, to a lesser extent, the uncertainties regarding the attenuation model of Liebe et al. (1993), we retained the value of 3.7 dB in the following steps of our study. The small variability obtained with the three sondes and the small differences with the simple model from Ulaby et al. (1981) seem to indicate that this attenuation correction is fairly accurate, resulting in a final radar calibration that is probably better than the expected 1–2 dBZ.

b. *Comparison of measured σ_0 with theoretical models*

The value of σ_0 at the sea surface is a function of radar wavelength, radar beam incidence angle, polarization, ocean surface wind speed, and surface wind direction. For incidence angles smaller than 15°, σ_0 is dominated by large-scale surface waves and at microwave frequencies the quasi-specular scattering theory has been shown to work well in this region. Theoretical values of σ_0 are calculated using Eq. (4) of Li et al. (2005) for the three different mean square surface slope models proposed in this paper: Cox and Munk (1954), Wu (1972, 1990), and Freilich and Vanhoff (2003). These theoretical values are then compared with the measurements performed with the RASTA radar.

As shown in Fig. 1, the two segments B–C and D–E of flight 78 were dedicated to the measurement of σ_0 at different incidence angles (computed as a combination of pitch and roll) with the radar slowly scanning ±20° across the flight track (this was achieved by the pilot, since the radar has no scanning capabilities). It has to be mentioned that the mounting angle errors of the antenna were taken into account for the computation of the incidence angle.

Figure 3 shows the σ_0 values measured with the RASTA radar at different incidence angles. Since on this flight the RASTA radar sampled only at 0.66 Hz, it has been chosen to cumulate all of the measurements (gray crosses in Fig. 3) for each segment. Then, the means and standard deviations for the different incidence bins are computed (black and dashed black lines in Fig. 3). This mean curve can be compared with the theoretical models, keeping in mind that the near-surface winds as given by the dropsondes were 6 and 9 m s^{-1} for segments B–C and D–E, respectively, explaining why the two segments have been separated in Fig. 3. The obtained mean curves compare well with the theoretical models up to 15° incidence angle, suggesting a proper calibration of the RASTA radar. This type of calibration check against the ocean surface is about to become a standard procedure and is currently used to evaluate the calibration of spaceborne radars such as

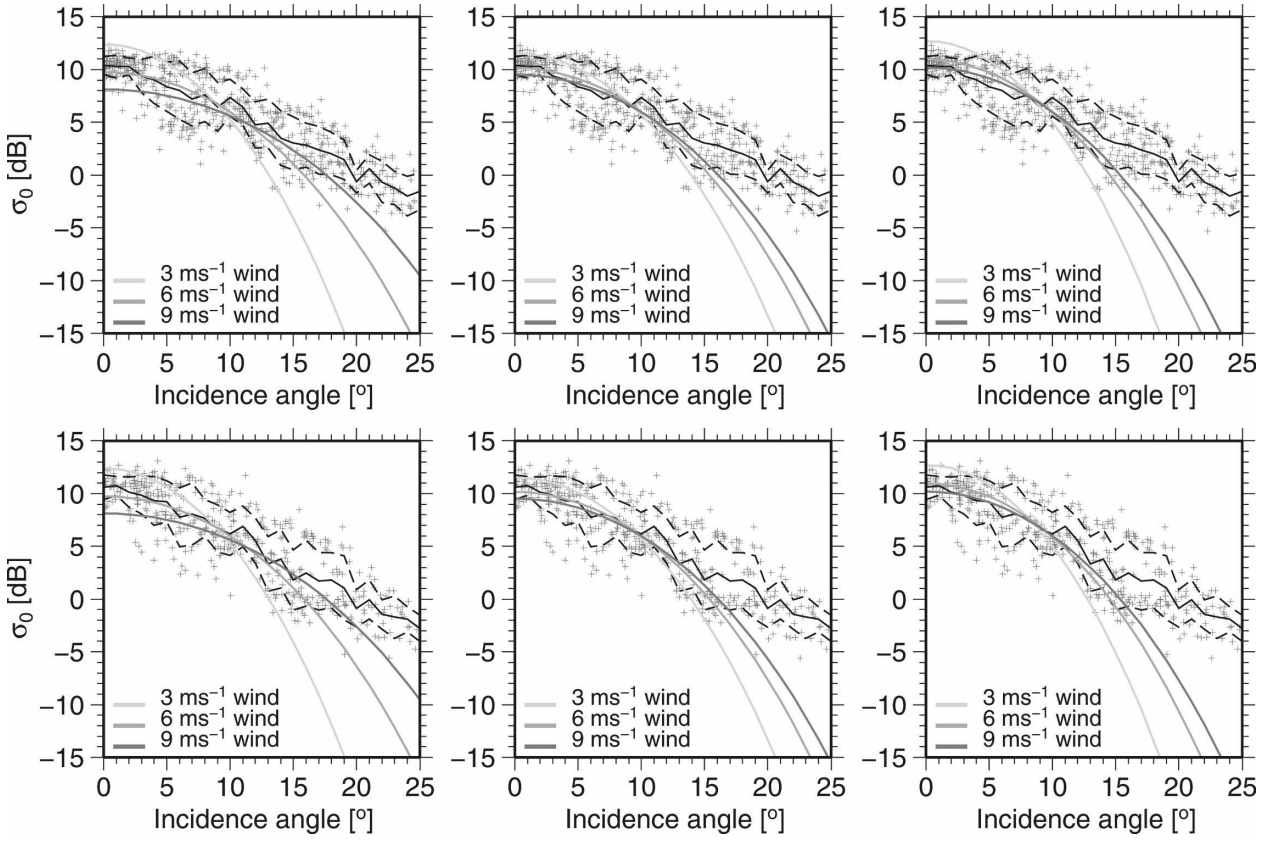

FIG. 3. The value of σ_0 (dB) measured by RASTA as a function of incidence angle (°) for the B–C (first line) and D–E (second line) segments compared to the quasi-specular model with 3, 6, and 9 ms^{-1} wind speeds of Cox and Munk (1954), Wu (1972, 1990), and Freilich and Vanhoff (2003) from left to right. The models are shown in solid gray lines; see legends. Each gray cross depicts a RASTA measurement and the solid and dashed black lines show the mean and the mean ±1 std dev of σ_0 at a given incidence.

for the precipitation radar on board the Tropcal Rainfall Measuring Mission (TRMM) (Okamoto et al. 2002) and for the *CloudSat* profiling radar. This figure also exhibits a slight reduction in the spread of the σ_0 value at about 10° incidence, in agreement with the findings at other frequencies, for instance 13.8 HGz (TRMM profiling radar frequency), where the ocean surface σ_0 under rain-free conditions is around 7 dB and has a minimum sensitivity to the wind speed near 10° incidence (see, e.g., Durden et al. 2003). The two dashed lines in Fig. 3 correspond to the mean value (solid black line) ±1 standard deviation. In this case the standard deviation is about 1.7 dB, suggesting a calibration of the RASTA radar with an accuracy comparable to that of the *CloudSat* radar [1–2 dB; Stephens et al. (2002)], implying that the comparisons performed in the following section are conducted with relatively well-calibrated radars.

This evaluation of the RASTA measurements by the nadir-looking antenna will be considered to be the reference in the following. The second step is to calibrate the zenith-looking antenna of RASTA with the previously calibrated nadir-looking antenna. Differences are expected between the antennas because of different loses within the waveguides. To do so, we directly compare the reflectivities of the nearest radar gates in the five directions to the nadir direction and assume that they should be statistically equal. For this purpose, all the data collected during the AMMA experiment have been cumulated, thus mixing different meteorological conditions (cirrus, deep convective cloud, etc.) and different flight altitudes. As expected, a roughly constant difference is found as a function of the nadir incidence reflectivity for all of the antennas, except at small signal-to-noise ratios (not shown). Statistically, we obtain a 2.3-dB difference between the nadir and zenith antennas (the zenith antenna being more sensitive than the nadir one). Using these calibration constants, the corresponding sensitivities of the RASTA radar at 1 km are −6.65 dB for the nadir-looking antenna and −8.97 dB for the zenith-looking antenna. It is to be noted that these sensitivity values are not sufficient for the inves-

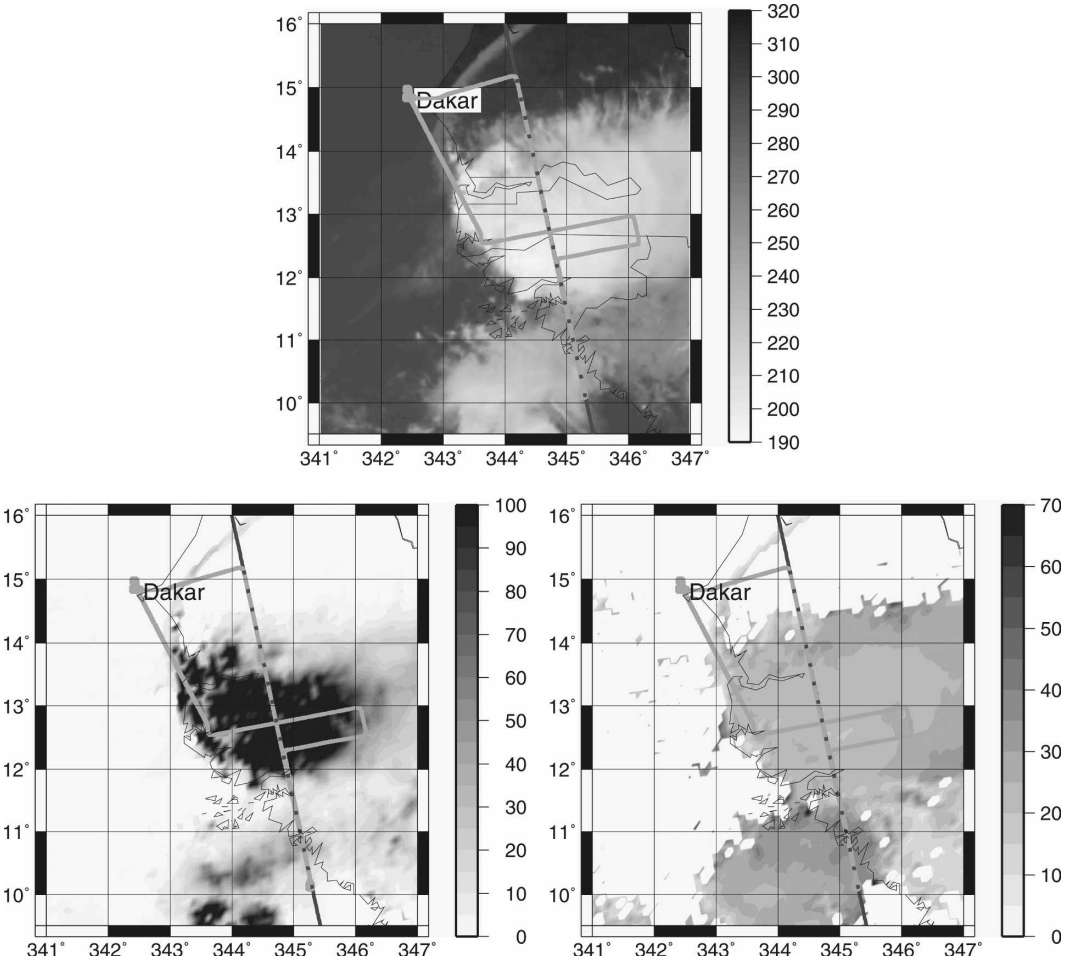

FIG. 4. (top) Meteosat IR channel brightness temperature (K), (bottom left) MODIS optical thickness, and (bottom right) MODIS effective radius (μm) at 1430 UTC on 22 Sep 2006 with the A-Train track (dark gray) and F-F20 flight track during flight 72 superimposed.

tigation of nonprecipitating clouds and have already been greatly improved since AMMA by the use of a new acquisition system (the final version was not available for AMMA) and by a better integration in the aircraft (15 dB have been easily gained here). Nevertheless, this sensitivity should be sufficient for the investigation of the ice anvils of mesoscale convective systems.

3. Comparisons of *CloudSat* and RASTA measurements

In the early morning (about 0600 UTC) of 22 September 2006 several decaying small-scale cells originating from disorganized convection merged (at the border between Mali and Guinea) in order to give birth to a more active cloud system. This system propagated westward over Senegal during the morning and reached southeast of Dakar at about 1430 UTC where it was sampled by the A-Train. It continued to propagate westward and arrived over the ocean about 2000 UTC where it decayed rapidly. It was the target of AMMA flight 72. Figure 4 shows the horizontal structure of the cloud system as observed by Meteosat in the 10.8-μm channel (IR) over Senegal at 1430 UTC at the same time as the cloud parameters (optical thickness and effective radius) derived from the Moderate Resolution Imaging Spectroradiometer (MODIS) on board *Aqua*, which was passing over the region at that time. The aircraft trajectory of the F-F20 during flight 72 is shown in light gray, and the A-Train ground track in dark gray.

During flight 72 the Falcon 20 flight plan consisted of an underflight of the *CloudSat* track (A–B segment in Fig. 5) and then a cross-track documentation. As a consequence of the differences in speed of the two platforms, the time necessary to sample the A–B segment is

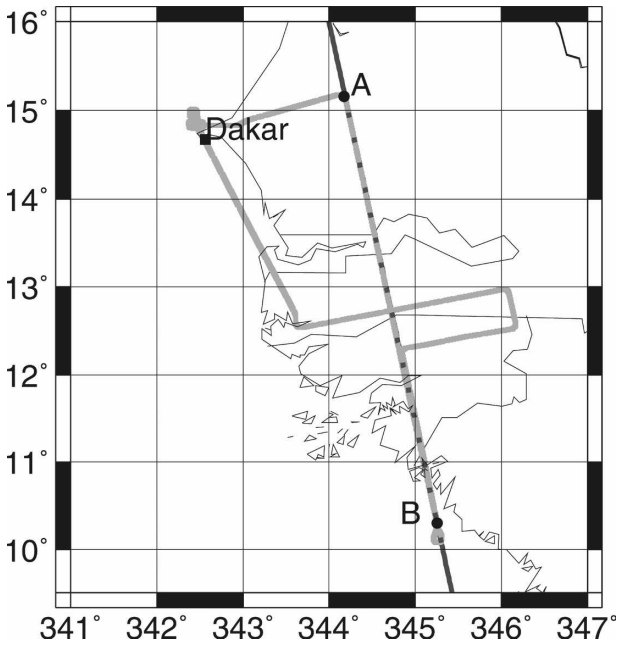

FIG. 5. Flight track on 22 Sep 2006. Light gray shows the aircraft track while dark gray shows the A-Train track.

about 1 min 20 s for the A-Train and 50 min for the F-F20. The flight plan has then been designed in order to optimize the coincidence in the middle of the A–B segment. As a result, increasingly larger differences are expected closer to A and B due either to the propagation of the meteorological system or changes in its internal organization. Along the A–B leg, it can be observed that this cloud system is relatively deep (very high optical thickness values in Fig. 4) and that it seems to be reasonably homogeneous horizontally (no strong horizontal gradients in the Meteosat image nor in the effective radius as observed by MODIS). We therefore expect a very small little beam-filling effect for both the *CloudSat* and RASTA radars in the along-track and cross-track directions.

Figure 6 shows the reflectivity measured along segment A–B by the *CloudSat* (top) and RASTA (bottom) radars, respectively. The white line in the RASTA picture corresponds to the F-F20 flight level. Near the aircraft, the area without observations corresponds to the four first radar gates for which RASTA does not provide reliable measurements (receiver is obstructed during emission). This flight has been performed in the stratiform region of a mesoscale convective system, above a rain region as can be observed in Fig. 6 with the melting layer (so-called radar bright band) located at about 4.5-km altitude. In the region above the melting layer the injection of significant amounts of liquid water may be expected as described in the conceptual scheme of Houze and Betts (1981). The *CloudSat* and RASTA reflectivity profile between the melting layer and the F-F20 flight level is somewhat puzzling, since it does not correspond to our current understanding of cloud microphysics. Indeed, as it is classically observed using ground-based precipitation radars, this reflectivity profile should be characterized by a negative reflectivity gradient in the vertical, owing to the aggregation process that acts to produce an increase in the size of the ice aggregates while falling down in the ice part, and therefore smaller particles in the upper part, larger particles as one approaches the melting layer. Since radar reflectivity is mostly sensitive to particle size (proportional to D^6 in a Rayleigh scattering regime), this configuration should correspond to a negative reflectivity gradient in the vertical. In our opinion, this decrease in reflectivity observed for the two radars in this region can only be due to attenuation. Nevertheless, even at 95 GHz it is not expected that pristine ice and ice aggregates produce significant attenuation (Hogan and Illingworth 1999). As an illustration, Li et al. (2001) estimated the attenuation profile associated with a tropical disturbance. They found an average two-way extinction rate of 0.38 dB km^{-1} within the ice cloud and 4.8 dB km^{-1} within moderate rain. This large observed attenuation can only be attributed to liquid water or to ice hydrometeors with very high density (like graupel or hail), which by providing both a highly scattering environment and an optically thick layer can result in a high scattering optical thickness (Battaglia et al. 2006b). Even if further investigations into the outputs of the in situ microphysics sondes are needed, supercooled water was indeed observed at the flight level with droplets reaching 25–30 μm in diameter. Some freezing occurred on the 2D sondes during this flight because of the presence of this supercooled water; however, when measurements were taken, they showed ice particles with a high degree of riming.

Going back to Fig. 6, the difference in the sensitivities of the two radars appears immediately, with for instance a cloud top observed at about 16 km for the *CloudSat* radar (the expected detection threshold for *CloudSat* being around -29 dBZ) and at about 13 km for the RASTA radar. Another interesting pattern is that, generally speaking, for all the time series the reflectivities measured by the *CloudSat* radar seem larger than those measured by the RASTA radar despite the fact that both radars are expected to be calibrated to within 1–2 dBZ (Stephens et al. 2002 for *CloudSat* and section 2 for RASTA). These differences in reflectivity cannot be attributed to errors in the collocation of the data since both instruments do clearly detect the same

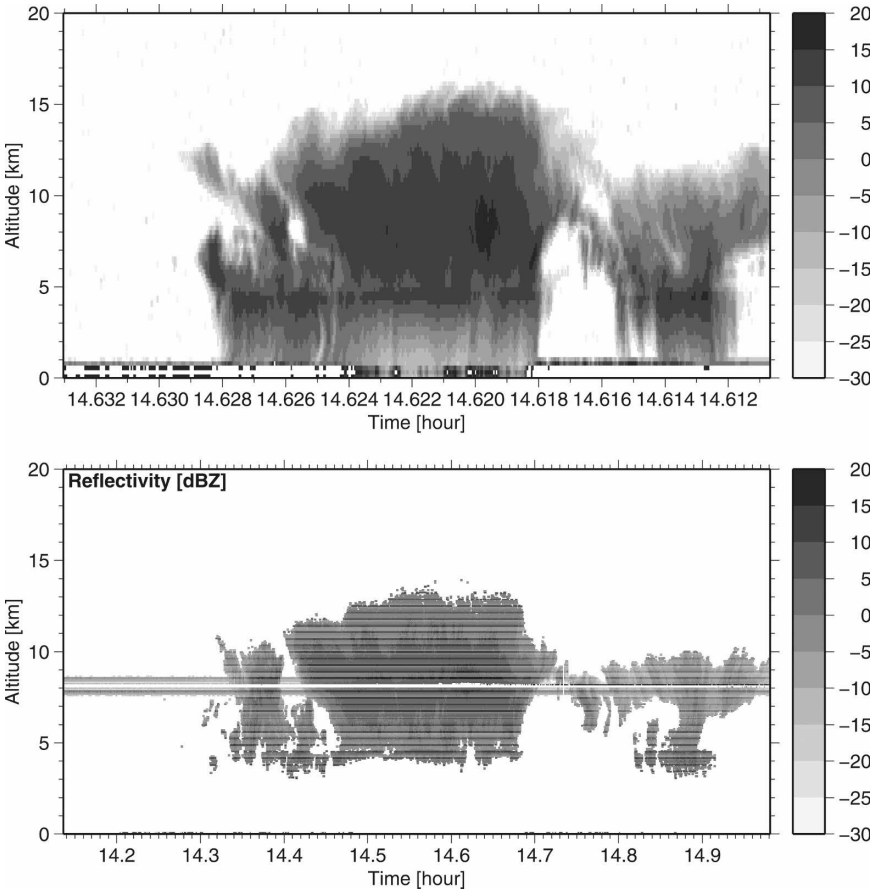

FIG. 6. Reflectivity (dBZ) measured by the (a) *CloudSat* radar (level 1B-CPR) and (b) by the nadir- and zenith-looking antennas of the RASTA radar along segment A–B. The white line at about 8-km altitude corresponds to the F-F20's flight altitude. The vertical cross section is presented in such a way that north is on the left-hand side of the picture; south is on the right-hand side.

cloud structure, even the small-scale structures. In addition, at the point of exactly coincident measurements of the two radars (14.6197 h at the latitude 12.275°) this difference still shows up. The good coincidence of the two instruments sampling can also be observed in Fig. 7 (for two different flight levels) where the two reflectivity measurements have been precisely geolocated as a function of latitude (the reason for regridding the data as a function of latitude is that small variations in the aircraft speed may cause an irregular sampling in terms of distance in a given direction) along the A–B leg. The small-scale structures are well observed in the two time series at the same location.

In this case the RASTA radar is flying within the ice anvil; therefore, its measurements close to the aircraft (8.42-km altitude; Fig. 7, bottom) should not be affected by attenuation while *CloudSat* may be affected at least by the path-integrated attenuation from cloud top down to 8.12-km altitude (flight altitude of the F-F20). Still, it is striking to observe that even at this flight altitude the *CloudSat* reflectivities remain as high as the RASTA reflectivities in the anvil core and are slightly smaller at the cloud border, suggesting that attenuation is no longer occurring (or decreasing) in the *CloudSat* radar measurements. Farther south (right-hand side in Fig. 7) the discrepancies between the two signals increase (even if the same broad structures are found in both radars) at the same time as the errors in the temporal collocation of both measurements (the exact collocation being shown by the vertical dashed line in Fig. 7).

The top panel in Fig. 7 shows the same time series but for a higher altitude (11 km). In this case (highest altitude for which a long time series is still measured by the RASTA radar), the RASTA radar reflectivity is much smaller than the *CloudSat* reflectivity, which is consis-

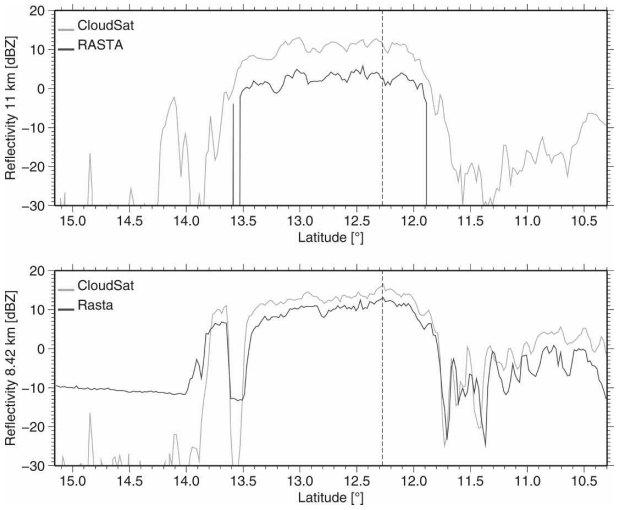

FIG. 7. Time series of reflectivity (dBZ) at (top) 11- and (bottom) 8.42-km altitude measured by the RASTA radar in dark gray and the *CloudSat* radar in light gray during flight 72. The lower axis corresponds to the latitude axis on which both measurements have been accurately collocated (north is on the left-hand side). The vertical dashed line shows the exact collocation of both radars (*CloudSat* moving northward; Rasta southward).

tent with the hypothesis of attenuation by the anvil cloud layer between 8.42 and 11 km. As seen in the mean vertical profile of the difference between the two reflectivities (Fig. 8), this difference remains roughly constant above 10.5 km, which strongly suggests that the *CloudSat* and RASTA reflectivities are not attenuated by the cloud layer above 11 km. As a result, the difference observed at 11 km corresponds to a direct estimate of the path-integrated attenuation of the RASTA reflectivities by the cloud layer. Interestingly, in the absence of any other effect, the same difference should be found but with opposite sign at 8.42-km altitude, with the *CloudSat* reflectivity being smaller than the RASTA reflectivity this time. As discussed just above, this is not what we observe. This puzzling situation is discussed below.

An explanation for the *CloudSat* reflectivity values larger than expected at 8.42 km is most likely the multiple scattering contamination in the spaceborne radar beam. This effect has been recently identified as an issue to be addressed for spaceborne radars at frequencies higher than 35 GHz (Marzano et al. 2003; Battaglia et al. 2005; Kobayashi et al. 2005) at high scattering optical thickness (defined as the columnar integral of the scattering coefficient), for example, associated with large amounts of high-density ice particles (Battaglia et al. 2007). Battaglia et al. (2007) show that if only single scattering is considered in a case of attenuation (as is observed in Fig. 6), some regions close to the ground should not be detectable since the signal falls below the minimum detection threshold of the radar whereas they are detectable when the multiple scattering is considered. In the *CloudSat* configuration for cold-front cases, Battaglia et al. (2007) estimate multiple scattering effects as high as 10 dB, 3 km above the melting layer in a deep snow layer leading to moderate rainfall rates at the ground (e.g., 28.2 or 6 mm h^{-1}). The contribution of multiple scattering enhancement becomes even larger when penetrating deeper into the cloud. These values are expected to be even larger in a case of a deep convective system such as that described in Battaglia et al. (2006b) where a large amount of graupel exists in the cloud shield and produces large rainfall rates. In the case of airborne radar systems characterized by a much smaller beamwidth than the *CloudSat* radar (0.7° in the case of RASTA), the reflectivity enhancement due to multiple scattering is always smaller than 1–2 dB in the simulations of Battaglia et al. (2007).

Another demonstration of multiple scattering enhancement (even if not providing an estimate of the magnitude) in this case may be obtained by looking at the radar gate at and below the surface level. Indeed, it is stated by Battaglia and Simmer (2008) that "smooth" profiles at the surface range are distinctive signatures of strong multiple scattering effects. For geolocation purposes, Fig. 6 has been limited to ground level but it can however be observed that the ground echo disappears in several occasions below the deep cloud anvil. In Fig. 8 the vertical axes has been kept up to −2 km in order to highlight in mean profiles what happens below the surface level.

A quantitative assessment of this multiple scattering effect in the *CloudSat* measurements can be performed at the F-F20 flight level if we assume that multiple scattering is negligible in the airborne radar beam, or rather translates into an error of about 1 dB in our *CloudSat* multiple scattering estimate. To do so, the reflectivity measured by *CloudSat* at the same altitude as the first usable gate of the RASTA radar (8.42-km height), $Z^{\mathrm{MS}}_{\mathrm{CloudSat}}$, can be rewritten as follows:

$$Z^{\mathrm{MS}}_{\mathrm{CloudSat}}(8.42) = Z^{\mathrm{SS}}_{\mathrm{CloudSat}}(8.42) + \Delta\, Z^{\mathrm{MS}}_{\mathrm{CloudSat}}(8.42)$$

$$Z^{\mathrm{MS}}_{\mathrm{CloudSat}}(8.42) = Z_e(8.42) - A_{2-\mathrm{ways}}(705 \rightarrow 8.42) + \Delta\, Z^{\mathrm{MS}}_{\mathrm{CloudSat}}(8.42), \quad (1)$$

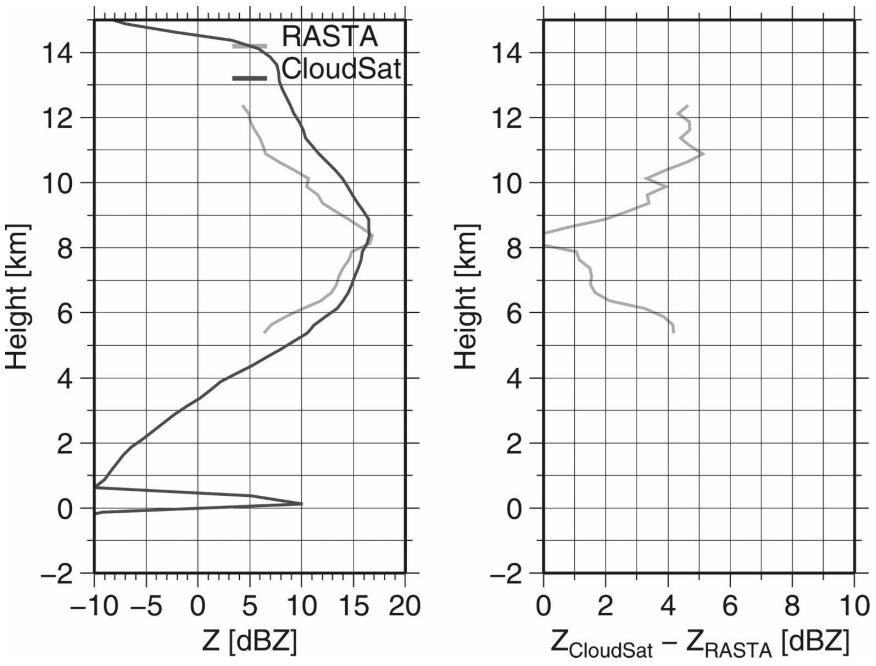

FIG. 8. Mean profiles of reflectivity from the RASTA (light gray) and *CloudSat* (dark gray) radars (a) in the vicinity of the exact coincident measurements and (b) differences in these mean profiles.

where $Z^{SS}_{CloudSat}$ is the corresponding single scattering *CloudSat* reflectivity, Z_e the equivalent reflectivity, and A_{2-ways} is the two-way attenuation along a given path (always positive). It is assumed that the attenuation of the RASTA radar between the flight level and gate 5 (i.e., 300 m) can be neglected. Therefore, the measurements of RASTA at this level correspond to a direct measurement of the equivalent reflectivity; that is, $Z^{MS}_{RASTA}(8.42) = Z_e(8.42)$.

As discussed previously, the right panel in Fig. 8 indicates that the layer above 10.5-km altitude does not produce significant attenuation, since between 10.5 and 12.5 km the difference between the two signals remains within 1 dB. We can therefore reasonably assume that the *CloudSat* measurements are unaffected by attenuation and multiple scattering at 11 km, which then implies that *CloudSat* provides a direct measurement of the equivalent reflectivity at this level; that is, $Z^{MS}_{CloudSat}(11) = Z_e(11)$. On the other hand, at this level the RASTA radar is affected by the path-integrated attenuation between 8.42 and 11 km, which can be rewritten as follows:

$$Z^{MS}_{RASTA}(11) = Z^{SS}_{RASTA}(11) = Z_e(11) - A_{2\text{-ways}}(8.42 \rightarrow 11). \quad (2)$$

If one makes the assumption that $A_{2\text{-ways}}(705 \rightarrow 8.42) = A_{2\text{-ways}}(11 \rightarrow 8.42) = A_{2\text{-ways}}(8.42 \rightarrow 11)$, which should be very accurate $A_{2\text{-ways}}$, then by recombining (1) and (2), we can finally write the following expression for the multiple scattering:

$$\Delta Z^{MS}_{CloudSat}(8.42) = Z^{MS}_{CloudSat}(8.42) - Z^{MS}_{RASTA}(8.42) + Z^{MS}_{CloudSat}(11) - Z^{MS}_{RASTA}(11). \quad (3)$$

From the mean vertical profile of $Z^{MS}_{CloudSat} - Z^{MS}_{RASTA}$ in Fig. 8, mean differences of -0.25 dB and 4.70 dB are found at the 8.42- and 11-km heights, respectively. The value of 4.7 dB can therefore be proposed as our estimate of the integrated attenuation by the cloud layer located between 8.42- and 11-km altitude. Using (3), the contribution of multiple scattering to $Z^{MS}_{CloudSat}$ at 8.42-km altitude can then be estimated as 4.5 dB. This value is directly contaminated by any error in the radar calibrations, the attenuation by atmospheric gases, and the assumptions made. An overall standard deviation of 2 dB is believed to be representative of the errors on these calculations. Therefore, the multiple scattering effect estimated in this West African anvil is 4.5 ± 2 dB. As an illustration of how an error in the calibration of one of the two radars translates into a contribution to the multiple scattering, we can show from Eq. (3) that, for instance, a *CloudSat* or RASTA reflectivity calibration error of 1 dBZ (which is small given that two radars have been calibrated independently from each other) leads to an overestimation of the multiple scat-

tering effect of 2 dB. It is therefore probably more realistic to conclude here that a multiple scattering effect of *at least* 2.5 dB has been found in the present paper.

Former studies have investigated quantitatively the multiple scattering contribution to the radar signal. In an idealized configuration (plane wave incident upon a slab of point scatterers), Tsang and Ishimaru (1985) provide an estimate of this enhancement, which can be corrected using the Kobayashi et al. (2005) estimation considering spherical waves and an antenna pattern. Battaglia et al. (2006a) show, using a Monte Carlo code, that they were able to obtain comparable results to Kobayashi et al. (2005). They then applied their radar signal simulator (including multiple scattering enhancement) to various "realistic" meteorological situations simulated with a mesoscale model, which are illustrated for the *CloudSat* configuration in Battaglia et al. (2007). Unfortunately, in this paper no detailed profiles of tropical cases are shown and substantial differences in the microphysical profiles may be expected between the midlatitude cases and the AMMA case. However, the values obtained from Fig. 12 in Battaglia et al. (2007) are in the same range as the ones obtained in our observational study. For instance, Battaglia et al. obtain an extinction coefficient of 0.3 km^{-1} at 4-km altitude corresponding to a multiple scattering enhancement as high as 3.5 dB, while we estimate this effect to be at least 2.5 dB.

Furthermore, it is possible to derive the vertical profile of the multiple scattering below the aircraft's flight altitude, since the RASTA and *CloudSat* reflectivities below the aircraft (measurements of the nadir antenna) should be attenuated in the same way from this altitude downward into the cloud. Any difference (once the integrated attenuation in the layer above the flight altitude is corrected in the *CloudSat* reflectivity) is then a direct measurement of the multiple scattering. Going back to Fig. 8 (right), this means that the vertical profile of the difference + 4.7 dB is the vertical profile of the multiple scattering, leading to a maximum value of at least 6.7 dB (8.7 dB in Fig. 8 minus the estimated calculation error of around 2 dB) of the multiple scattering enhancement, 1 km above the melting layer.

The development of methods to correct for multiple scattering in the *CloudSat* reflectivities is therefore needed to ensure a good level of accuracy in the operational and research products that are derived in mesoscale convective systems [including ice water contents (IWCs), rainfall rates, and heating fluxes] from the *CloudSat* measurements, even if its effect is only expected for very optically thick clouds. If we refer to the values obtained previously from the RASTA and *CloudSat* measurements (a 4.7-dB integrated attenuation and at least a 2.5-dB multiple scattering contamination) for a *CloudSat* effective reflectivity of 16.53 dBZ, and if the Liu and Illingworth (2000) relationship at 95 GHz is applied at the aircraft flight level to the *CloudSat* reflectivities that are not corrected and corrected for multiple scattering, then IWCs are about 3.17 and 2.19 gm^{-3}, corresponding to at least 144% fractional error. This result should be taken with caution, obviously, since the Liu and Illingworth (2000) statistical relationships have been built for nonprecipitating clouds. This figure is merely given here as an illustration of the potential errors that could arise from using simple IWC–Z relationships or methods relying on radar reflectivity alone, which is the case of the standard *CloudSat* 2B-CWC product.

4. Conclusions

The AMMA experiment, which took place in West Africa between June and September 2006, was one of the first opportunities to evaluate the *CloudSat* radar products. In this paper an evaluation of the level 1 product (i.e., calibrated reflectivity) has been proposed thanks to coincident measurements performed with a five-beam airborne 95-GHz Doppler radar (RASTA).

To make sure that the measurements of the two instruments are directly comparable, an evaluation of the RASTA calibration was first performed against the ocean surface following the method proposed by Li et al. (2005). The surface backscattering cross section measured by the RASTA radar during flight 78 (28 September 2006) was found to correctly reproduce the theoretical models proposed in the literature for the range of surface winds encountered and can then be assumed to be calibrated within a 1–2-dB range as stated in Li et al. (2005) regarding this calibration method. An estimation of the RASTA sensitivity was also provided and appears as a major issue for comparison with the *CloudSat* radar (limiting the comparison to the very thick ice anvil region). However, improvements in the acquisition system are about to overcome this limitation.

During flight 72 (22 September 2006) RASTA flew under the *CloudSat* track, thereby acquiring coincident measurements. A direct comparison at two different flight levels was performed in the deep ice anvil of the sampled mesoscale convective system. Several interesting features are found. First, significant integrated attenuation, as large as 4.7 dB for a 2.5-km layer is clearly observed in the ice anvil. Then at flight level, the

CloudSat reflectivities remain as high as the RASTA reflectivities, although we would expect them to be smaller owing to attenuation, which is suggestive of the presence of multiple scattering in the *CloudSat* radar beam. By stating that the two radars are affected by the same attenuation along the same given path, this contribution of multiple scattering to the measured *CloudSat* reflectivity has been quantified at a given height within the ice anvil, and is found to be at least 2.5 dB. Furthermore, as one approaches the melting layer, in a region in which there is a much larger amount of supercooled water, this multiple scattering is found to be of at least 6.7 dB. Finally, the need for taking this contribution into account in level 2 *CloudSat* products is highlighted.

By flying within the cloudy region and sampling simultaneously upward and downward, the RASTA radar has demonstrated that this flight strategy is suitable in order to estimate the multiple scattering enhancement profile below the flying altitude. Obtaining more observational datasets (sampling up to the rain region thanks to improved sensitivity) is of considerable interest in order to provide estimates of the spaceborne radar multiple scattering enhancements in different meteorological situations comparable to the theoretical studies.

Acknowledgments. The *CloudSat* data were obtained from the *CloudSat* Data Processing Center, and the NASA *CloudSat* Project is acknowledged. Based on a French initiative, AMMA was built by an international scientific group and is currently funded by a large number of agencies, especially from France, the United Kingdom, the United States, and Africa. It has been the beneficiary of a major financial contribution from the European Community's Sixth Framework Research Programme. Detailed information on scientific coordination and funding is available from the AMMA International Web site (http://www.amma-international.org).

The authors are also grateful to Emmanuel Moreau from Novimet for useful discussions regarding multiple scattering in the *CloudSat* measurements and to Michel Chong from Laboratoire d'Aérologie for the processing of the dropsonde data. Finally, we also wish to thank the F-F20 pilots (Daniel Damien and Jean-Luc Pilotto) for their skillful ±20° roll at constant pitch.

REFERENCES

Battaglia, A., and C. Simmer, 2008: How does multiple scattering affect the spaceborne W-band radar measurements at ranges close to and crossing the surface-range? *IEEE Trans. Geosci. Remote Sens.,* **46,** 1644–1651.

——, M. O. Ajewole, and C. Simmer, 2005: Multiple scattering effects due to hydrometeors on precipitation radar systems. *Geophys. Res. Lett.,* **32,** L19801, doi:10.1029/2005GL023810.

——, ——, and ——, 2006a: Evaluation of radar multiple-scattering effects from a GPM perspective. Part I: Model description and validation. *J. Appl. Meteor. Climatol.,* **45,** 1634–1647.

——, ——, and ——, 2006b: Evaluation of radar multiple-scattering effects from a GPM perspective. Part II: Model results. *J. Appl. Meteor. Climatol.,* **45,** 1648–1664.

——, ——, and ——, 2007: Evaluation of radar multiple scattering effects in *CloudSat* configuration. *Atmos. Chem. Phys. Discuss.,* **7,** 1719–1730.

Cox, C., and W. Munk, 1954: Measurements of the roughness of the sea surface from photographs of the sun's glitter. *J. Opt. Soc. Amer.,* **144,** 838–850.

Durden, S. L., Z. S. Haddad, and L. Li, 2003: Comparison of TRMM Precipitation Radar and airborne radar data. *J. Appl. Meteor.,* **42,** 769–774.

Ellingson, R. G., J. Ellis, and S. Fels, 1991: The intercomparison of radiation codes used in climate models: Long wave results. *J. Geophys. Res.,* **96** (D5), 8929–8953.

Freilich, M. H., and B. A. Vanhoff, 2003: The relationship between winds, surface roughness, and the radar backscatter at low incidence angles from TRMM precipitation measurements. *J. Atmos. Oceanic Technol.,* **20,** 549–562.

Hogan, R. J., and A. J. Illingworth, 1999: The potential of spaceborne dual-wavelength radar to make measurements of cirrus clouds. *J. Atmos. Oceanic Technol.,* **16,** 518–531.

Houze, R. A., and A. K. Betts, 1981: Convection in GATE. *Rev. Geophys. Space Phys.,* **19,** 541–576.

Kobayashi, S., S. Tanelli, and E. Im, 2005: Second-order multiple scattering theory associated with backscattering enhancement for a millimeter wavelength weather radar with a finite beam width. *Radio Sci.,* **40,** RS6015, doi:10.1029/2004RS003219.

Li, L., and Coauthors, 2001: Retrieval of atmospheric attenuation using combined ground-based and airborne 95-GHz cloud radar measurements. *J. Atmos. Oceanic Technol.,* **18,** 1345–1353.

——, G. M. Heymsfield, L. Tian, and P. E. Racette, 2005: Measurements of ocean surface backscattering using an airborne 95-GHz cloud radar—Implication for calibration of airborne and spaceborne W-band radars. *J. Atmos. Oceanic Technol.,* **22,** 1033–1045.

Liebe, H. J., G. A. Hufford, and M. G. Cotton, 1993: Propagation modeling of moist air and suspended water/ice particles below 1000 GHz. Preprints, *Electromagnetic Wave Propagation Panel Symp.,* Palma de Mallorca, Spain, AGARD Conf. Proc. 542.

Liu, C. L., and A. J. Illingworth, 2000: Toward more accurate retrievals of ice water content from radar measurements of clouds. *J. Appl. Meteor.,* **39,** 1130–1146.

Marzano, F. S., L. Roberti, S. Di Michele, A. Mugnai, and A. Tassa, 2003: Modeling of apparent radar reflectivity due to convective clouds at attenuating wavelengths. *Radio Sci.,* **38,** 1002, doi:10.1029/2002RS002613.

Okamoto, K., T. Kubokawa, A. Tamura, and T. Ushio, 2002: Long term trend of ocean surface normalized radar cross section observed by TRMM precipitation radar. *Proc. Second Global Precipitation Mission (GPM) International Planning Workshop,* Shinagawa, Japan, Communications Research Laboratory–National Space Development Agency of Japan–NASDA–NASA.

Protat, A., and Coauthors, 2004: Le Projet RALI: Combinaison d'un radar nuage et d'un lidar pour l'étude des nuages faiblement précipitants. *La Météor.,* **47,** 23–33.

Stephens, G. L., and Coauthors, 2002: The *CloudSat* mission and the A-Train. *Bull. Amer. Meteor. Soc.,* **83,** 1771–1790.

Testud, J., P. H. Hildebrand, and W.-C. Lee, 1995: A procedure to correct airborne Doppler radar data for navigation errors using the echo returned from the earth's surface. *J. Atmos. Oceanic Technol.,* **12,** 800–820.

Tsang, L., and A. Ishimaru, 1985: Theory of backscattering enhancement of random discrete isotropic scatterers based on the summation of all ladder and cyclical terms. *J. Opt. Soc. Amer.,* **2,** 1331–1338.

Ulaby, F. T., R. K. Moore, and A. K. Fung, 1981: *Microwave Remote Sensing, Active and Passive.* Vol. I. *Microwave Remote Sensing, Fundamentals and Radiometry,* Artech House, Inc.

Wu, J., 1972: Sea-surface slope and equilibrium wind-wave spectra. *Phys. Fluids,* **15,** 741–747.

——, 1990: Mean square slopes of the wind distributed water surface, their magnitude, directionality and composition. *Radio Sci.,* **25,** 37–48.